MARCEL DEKKER, INC. • 270 MADISON AVENUE • NEW YORK, NY 10016

APPLIED SPECTROSCOPY REVIEWS
Vol. 38, No. 2, pp. 133–153, 2003

Infrared Multispectral Imaging: Principles and Instrumentation

Chieu D. Tran*

Department of Chemistry, Marquette University,
Milwaukee, Wisconsin, USA

CONTENTS

*Correspondence. Chieu D. Tran, Department of Chemistry, Marquette University, P.O. Box 1881, Milwaukee, Wisconsin 53201-1881, USA; E-mail: chieu.tran@marquette.edu.

DOI: 10.1081/ASR-120021165 0570-4928 (Print); 1520-569X (Online)

ABSTRACT

A multispectral imaging spectrometer is an instrument that can simultaneously record spectral and spatial information of a samples. Chemical and physical properties of the sample can be elucidated from such images. In a multispectral imaging instrument, a camera is used to record the spatial distribution of the sample, and the spectral information is gained by scanning a dispersive device to record spectra for each image. This overview article describes operational principles and recent development of various components used in infrared multispectral imaging instruments including the electronic dispersive devices (acousto-optic tunable filter and liquid crystal tunable filter) and IR cameras (InGaAs, InSb, HgCdTe and QWIP cameras).

Key Words: Acousto-optic tunable filter; Liquid crystal tunable filter; Focal plane arrays; InGaAs; InSb; HgCdTe; Infrared; Imaging.

I. INTRODUCTION

Infrared multispectral imaging, sometimes referred to in literature as hyperspectral imaging, is a relatively recent development that combines the chemically rich information available from spectroscopy with the ability to acquire this information in a spatially resolved manner.[1] Multispectral images are acquired by an instrument that can simultaneously record spectral and spatial information of a sample, i.e., the recorded images contain signals that are generated by molecules or units in a sample plotted as a function of spectral and spatial distribution.[1] As such, a single data set consists of both spatial and spectral information. The typical dimensions of this data set range from 256×256 to 320×240 pixels, with each pixel containing a full IR spectrum. Such data will facilitate visualizing chemical distribution in a sample or chemical compositions of several samples. The type information is of particular importance since it is known that chemical as well as physical properties of materials are dependent on the chemical distribution within the samples. Instrumentally, in a multispectral imaging

instrument, an infrared camera is used to record the spatial distribution of the sample, and the spectral information is gained by scanning a dispersive device to record spectra for each image.[1] Dispersive devices based on mechanical scanning (e.g., filter wheels, monochromators) are not desirable because, in addition to their relatively large size (and hence impractical for field deployment) they are prone to vibrations and can only be spectrally tuned in a relatively narrow range with a relatively slow speed. Recent advances in material sciences, electronics and computer sciences have led to the development of novel types of electronically tunable filters. Acousto-optic tunable filters (AOTFs)[2–20] and liquid crystal tunable filters (LCTFs)[21,22] belong to these types of electronic tuning devices. They are particularly suited for use in multispectral imaging instruments since they contain no moving parts and can be spectrally tuned over a wide spectral range (from near infrared to middle infrared) with much faster speeds (from micro- to milliseconds).

Recent development in material science, optics, and electronics have also made it possible to acquire high performance cooled and uncooled infrared array detectors (also known as IR focal plance arrays (FPAs)) at relatively reasonable costs. FPAs based on various materials (InGaAs, InSb, HgCdTe, and QWIP) with different number of pixels (from 64×64 to 1024×1024 pixels) and different spectral detection range (from 1 to 12 μm) are now readily commercially available.[23–31]

Because of the recent developments in spectral tunable filters and IR cameras, many different types of IR multispectral imaging instruments have been developed in recent years and these instruments made it possible to perform studies and measurements which to date were not possible otherwise. In this overview, detailed information on operation principles, advantages and disadvantages of various types of electronic tuning devices (AOTFs, and LCTFs) and infrared cameras (InGaAs, InSb, HgCdTe, and QWIP focal plane arrays) will be described. Comparison of different near and middle-IR multispectral imaging systems will be made including some of their unique applications. It is noteworthy to add that this overview covers only multispectral imaging systems based on tunable filters, namely AOTFs and LCTFs. Fourier-Transform (FT) technique based on Michelson interferometer can also be used as dispersive device in multispectral imaging instruments. In fact, multispectral imaging instruments based on FT-Michelson interferometer have been developed[32–39] and commerically available from several manufactures. Multispectral imaging based on FT will not be covered in this overview because not only spectral tuning mechanism for the FT is distinctly different from those of the AOTFs

and LCTFs, but also it has been the subject of several reviews.[38,39] Other applications of AOTFs and LCTFs as spectral tuning device in a different imaging technique, namely Raman imaging,[40–42] will not be covered in this overview.

II. SPECTRAL TUNING DEVICES

1. Acousto-optic Tunable Filters

Theory and operational principles of an AOTF have been described in details in some recent excellent reviews.[5,18,20] Essentially, AOTF is an all-solid state, electronic dispersive device which is based on the diffraction of light in a crystal.[2,20] Light is diffracted by an acoustic wave because an acoustic wave when propagates in a transparent material will produce a periodic modulation of the index of refraction (via the elasto-optical effect). This, in turn, will create a moving grating which diffracts portions of an incident light beam. The diffraction process can, therefore, be considered as a transfer of energy and momentum. Conservation of the energy and momentum must therefore, be maintained. The equation for conservation of momentum can be written as:[2,20]

$$\mathbf{k_d} = \mathbf{k_i} \pm \mathbf{k_s} \tag{1}$$

where $\mathbf{k_i}$, $\mathbf{k_d}$, and $\mathbf{k_a}$ are the wave vector of the incident and diffracted light, and of the phonon.

In an AOTF, the acousto-optic interaction occurs in an anisotropic medium, and the polarization of the diffracted beam is orthogonal to that of the incident beam. The momenta of incident and diffracted photons are:

$$|\mathbf{k_i}| = 2\pi n_i/\lambda \tag{2}$$

$$|\mathbf{k_d}| = 2\pi n_d/\lambda \tag{3}$$

They are not equal since one is ordinary ray and the other is extraordinary ray (i.e., $n_i \neq n_d$).

In the case of collinear AOTF, the incident and diffracted light beams, and the acoustic beam are all collinear. If the incident light is an extraordinary and the diffracted light is an ordinary ray, the momentum matching condition becomes:

$$\mathbf{k_d} = \mathbf{k_i} - \mathbf{k_s} \tag{4}$$

$$f_s = v_s(n_e - n_o)/\lambda \tag{5}$$

where $|\mathbf{k_s}| = 2\pi f_s/v_s$ and f_s and v_s are the frequency and velocity of the acoustic wave. Equation (5) can be generalized for all types of AOTFs including the collinear and the noncollinear AOTFs:

$$f_s = [v_s(n_e - n_d)]\frac{1}{\lambda_o}(\sin^4\theta_i + \sin^2 2\theta_i)^{1/2} \tag{6}$$

where θ_i is the incident angle. When $\theta_i = 90^\circ$ Eq. (6) reduced to Eq. (5), i.e., the case of collinear.

It is thus, evidently clear that in an anisotropic crystal where the phase matching requirement is satisfied, diffraction occurs only under optimal conditions. These conditions are defined by the frequency of the acoustic waves and the wavelength of particular diffracted light. For a given acoustic frequency, only light whose wavelength satisfies either Eq. (5) or Eq. (6) is diffracted from the crystal. The filter can, therefore, be spectrally tuned by changing the frequency of the acoustic waves (i.e., f_s).

Generally, the AOTF is fabricated from an anisotropic crystal onto it an array of $LiNbO_3$ piezoelectric transducers are bonded. A ratio frequency (RF) signal is applied to the transducers which, in turn, generates an acoustic wave propagating through the TeO_2 crystal. These propagating acoustic waves produce a periodic moving grating which will diffract portions of an incident light beam. Figure 1A–C show collinear and noncollinear type AOTFs. As illustrated, a light beam propagating as an e-ray is converted into an o-ray by interaction with, and diffraction from, an acoustic wave propagating in the same medium. In a collinear type AOTF (Fig. 1A) the diffracted (o-beam) is separated from the transmitted beam (e-beam) by mean of a polarizer (analyzer). Since the diffracted beam is spatially separated from the transmitted beam in a noncollinear AOTF (Fig. 1 B and 1 C) it is not necessary to use an analyzer. As depicted in Eq. (6), for a fixed acoustic frequency and sufficiently long interaction length, only a very narrow band of optical frequencies can approximately satisfy the phase matching condition and be diffracted. The wavelength of the diffracted light can therefore, be tuned over large spectral regions by simply changing the frequency of the applied RF signal. Figure 2A and 2B show the spectral tuning curse of a noncollinear AOTF fabricated from TeO_2 for the visible and NIR region. As illustrated, light can be spectrally tuned from 400 to 700 nm and from 1.1 to 2.4 μm by simply scanning the frequency of the applied RF signal from 222 to 100 MHz and from 60 to 30 MHz, respectively.[2–20]

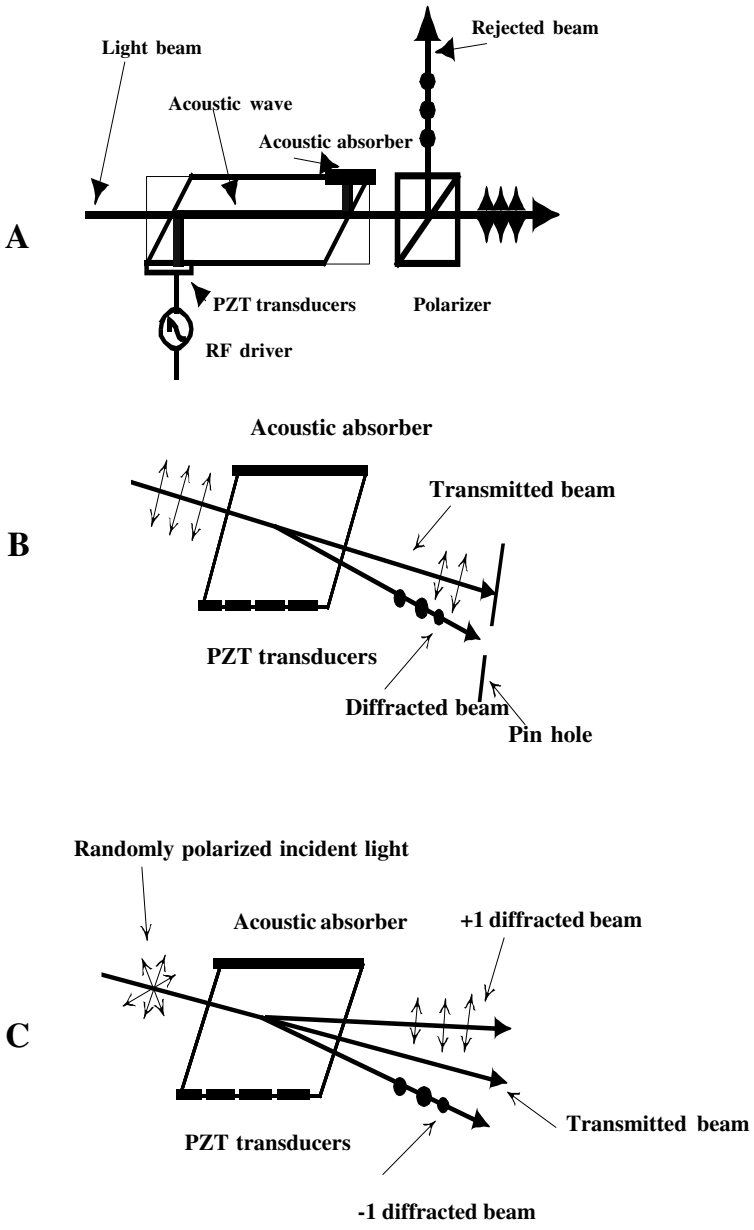

Figure 1. Different types of acousto-optic tunable filters (AOTF): (A) collinear AOTF; (B) noncollinear AOTF with polarized light incident light; and (C) noncollinear AOTF with randomly polarized light incident light.

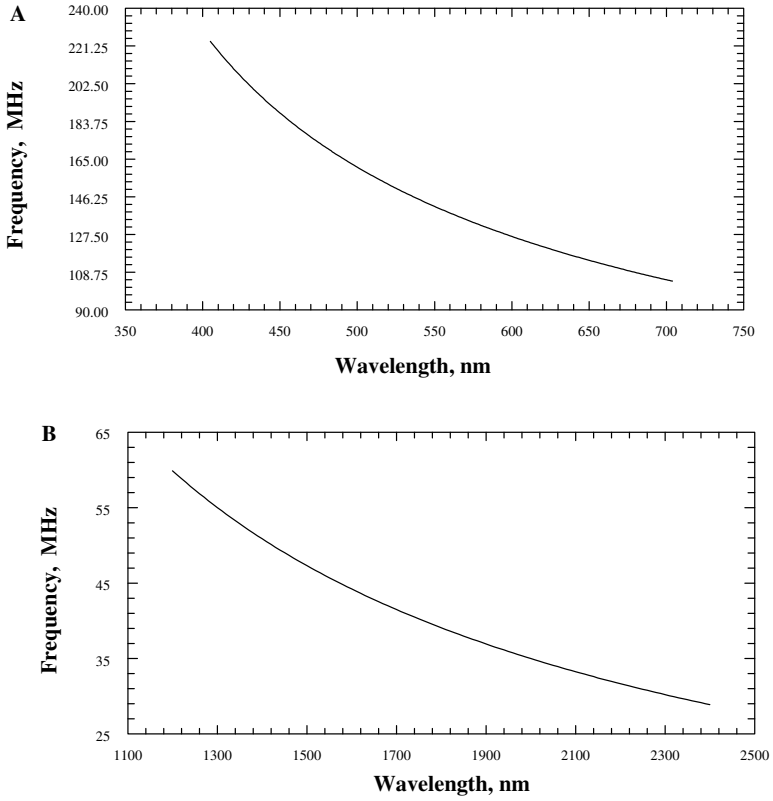

Figure 2. Spectral tuning curves of noncollinear TeO_2 AOTF for (A) the visible region and (B) for the near-infrared region.

Depending on the spectral region, different birefringent crystals are used to fabricate AOTFs. Three most widely used crystals for AOTFs are shown in Table 1. As illustrated, quartz is often used for AOTF in the UV and visible region.[10] Quartz is known to have relatively good optical transparency for UV and visible region. However, because it has a relatively low acoustic figure of merit (ability to couple acoustic wave to the crystal), AOTFs based on quartz often require, in addition to collinear configuration (to enhance acousto-optic interaction length l), relatively high power of applied RF signal. The high RF power consumption somewhat limits applications of the quartz based AOTFs.[10] In addition, the collinear configuration of this type of AOTF renders difficulty in using this

Table 1. Properties of different AOTF crystals.

Material	Transparency range, μm	Acoustic figure of merit
Quartz	0.2–4.5	1
TeO_2	0.35–5.0	795
Tl_3AsSe_3	1.0–16	900

type of AOTF in multispectral imaging instrument. Different from quartz, TeO_2 crystal is good for AOTF from the visible region up about 5 μm where it becomes opaque. Tl_3AsSe_3 (often known as TAS) can be used for AOTF from 1 to 16 μm. Because these two crystals have relatively higher acoustic figures of merit (795-fold and 900-fold higher than quartz), AOTFs based on these crystals require relatively lower power of applied RF and signal. It addition, they can be constructed using noncollinear configuration.[2–20] As a consequence, TeO_2 and Tl_3AsSe_3 based AOTFs are particularly suited for use in multispectral imaging instruments.

Of particular importance to the multispectral imaging technique is the scanning speed of the AOTF. The scanning speed of the filter is defined by the speed of the acoustic wave in the crystal, which is on the order of microseconds.[2–20] As a consequence, AOTFs have fastest scanning speed compared to other dispersive devices including conventional gratings, LCTFs and interferometers.

Spectral resolution ($\Delta\lambda$) of the AOTF is related to the wavelength of the diffracted light λ_0, acousto-optic interaction length l, incident angle θ_i and $\Delta n(= n_e - n_o)$ by:[2–20]

$$\Delta\lambda = \frac{\lambda_0^2}{2l\Delta \sin^2 \theta_i} \tag{7}$$

As depicted in the equation, the spectral resolution is proportional to the wavelength of diffracted light and inversely proportional to the interaction length. As a consequence, quartz collinear AOTFs for the UV often have high spectral resolution compared to noncollinear TeO_2 AOTFs for the visible, near- and middle-IR. Shown in Fig. 3 A–C are spectral resolution of a quartz collinear AOTF for the UV and visible region (Fig. 1A), the TeO_2 noncollinear AOTF for the visible (2B) and near-IR. As illustrated, spectral resolution of a few angstroms can be readily achieved with the quartz collinear AOTF for the UV region.

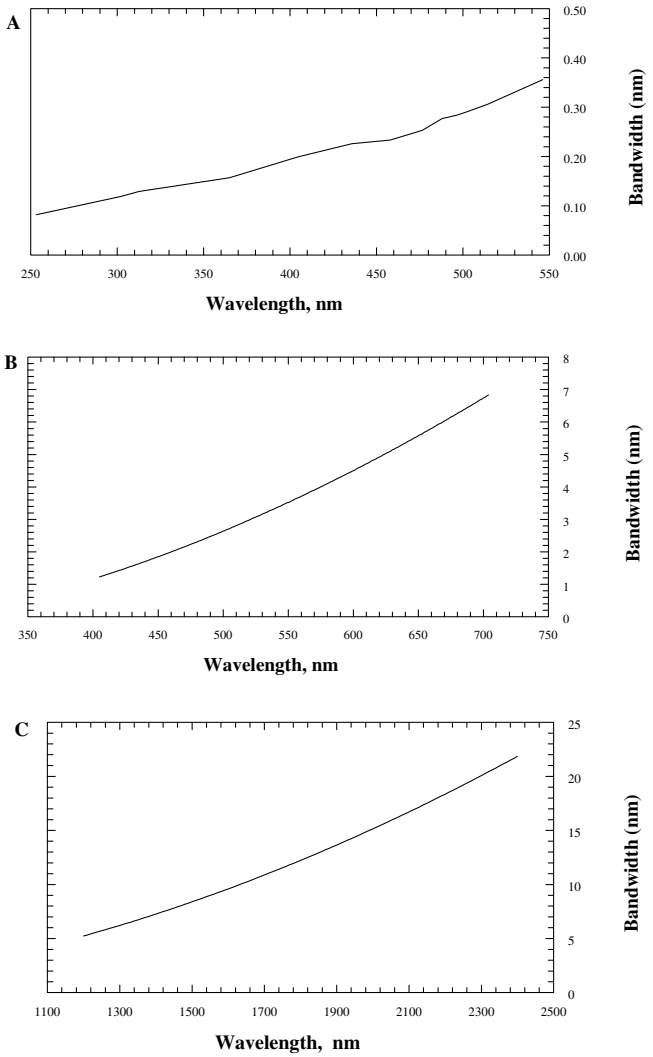

Figure 3. Spectral resolution of (A) collinear quartz AOTF for the visible and UV region; (B) noncollinear TeO_2 AOTF for the visible region; and (C) noncollinear TeO_2 AOTF for the near-IR region.

However, the resolution deteriorates somewhat in an AOTF with a noncollinear configuration fabricated from TeO_2 (up to a few nanometers) (3B). As wavelength becomes longer in the NIR, the spectral resolution increases to tens of nanometers (3C).

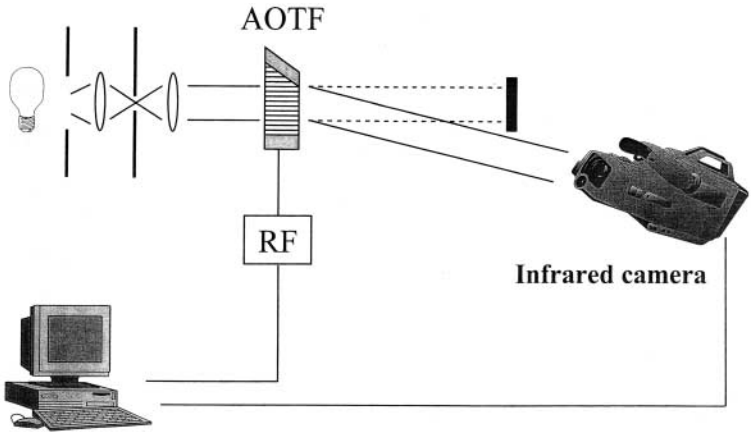

Figure 4. Schematic diagram of an infrared multispectral imaging instrument based on an acousto-optic tunable filter: AOTF, acousto-optic tunable filter; RF, RF signal generator.

Taken together, the AOTFs offer such advantages as being compact, all-solid state (contains no moving parts), having rapid scanning ability (microseconds), wide spectral tuning range (from visible to NIR and IR) and high throughput (> 90% diffraction efficiency for incident polarized light), allowing high speed random or sequential wavelength access, and giving high resolution (a few angstroms). As a consequence, AOTFs is particularly suited for use as a dispersive device in a multispectral imaging instrument. In fact, AOTF based multispectral imaging spectrometers have been developed for the near- and middle-IR. A schematic diagram of such instrument is shown in Fig. 4.[43–52] As illustrated, advantages of the AOTF provide not only the simplicity in construction of the instrument but also ease of operation. Features such as high sensitivity, fast scanning speed made it possible for this imaging spectrometer to be used for studies which are not possible with other (LCTS and interferometer based) imaging instruments.[43–52] These include the determination of inhomogeneity in the kinetics of curing of epoxy resins and kinetics and chemical inhomogeneity in the sol–gel formation.[43–52] Furthermore, because the AOTF based imaging spectrometer is compact, contains no moving parts and requires relatively low electrical power, it can be powered by a battery. As a consequence, it can be deployed directly in fields agricultural and environmental measurements.

2. Liquid Crystal Tunable Filters

Liquid crystal is a notch filter with a center wavelength that can be varied by changing the voltage that is applied onto the filter.[21,22] Specifically, it is based on a Lyot filter. In a Lyot filter, a birefringent crystal is placed between two polarizers whose axes are parallel to each other. The input polarizer converts incoming unpolarized light into linearly polarized light. The polarized light then passes through the birefringent crystal where it is split into ordinary and extraordinary beams. The birefringent crystal also introduces phase delay between the two beams (and hence, it is called a retarder). The optical path difference between the two beams, is known as a retardance Γ. For light with wavelength λ, the phase difference δ introduced by a retarder with a retardance Γ is given by:[21,22]

$$\delta = \frac{2\pi\Gamma}{\lambda} \tag{8}$$

The light coming out of the retarder then passes through a second polarizer (known as an analyzer). The intensity of the transmitted beam is dependent on $\cos^2\delta$. As a consequence, only light with certain wavelength can be transmitted. Specifically, light with wavelength for which $\Gamma = k\lambda$ will experience high transmittance while those for which $\Gamma = (k+1)\lambda$ will be extinguished. Generally, a Lyot filter is constructed by placing each quartz or calcite birefringent retarder in series with a liquid crystal variable waveplate. The liquid crystal waveplate is essentially an electrically variable retardance, which provides the means to spectrally tune the filter. The retardance of stage i give by:[21,22]

$$\Gamma = 2^i\lambda \tag{9}$$

Light of wavelength λ is transmitted without loss because it meets the transmission criteria for each stage, while light of other wavelengths is extinguished by one or more stages.

Because of the limited availability of materials which posses electro-optic properties necessary for construction of LCTFs, the longer wavelength which currently available LCTFs can only be spectrally tuned is 1700 nm. Furthermore, because of the properties of electro-optic materials used, the spectral tuning range of this type of filter is relatively narrower than those the AOTFs. Typically, a NIR LCTF cab be spectrally tuned from 1000 to 7000 nm. However, the narrowly tuning feature of the LCTFs should not restrict their applications in multispectral imaging instruments. This is because this tuning range (1000–1700 nm) match very well with the InGaAs focal plane arrays cameras for the NR region.

In addition, LCTFs have relatively large aceptance angle and are commercially available with relatively large apertures than AOTFs (NIR LCTFs are available with aperture as large as 20 mm). Because these features can somewhat compensate for the relatively lower transmission efficiencies of the LCTFs, these electro-optic tunable filters can be used for the construction of multispectral imaging instruments. In fact, multispectral imaging instruments based on LCTFs have been constructed and used for various types of important studies.[53,54] However, compared to AOTF based multispectral imaging instruments, LCTF based instruments cannot be used for measurements which required fast scanning speed. This is due to the fact that while the AOTFs can be spectrally scanned in microseconds, the fastest speed which LCTF can be tuned is only milliseconds. The slower speed of the LCTFs are due to the slower electro-optical responses of the materials used to construct the filters.

III. INFRARED FOCAL PLANE ARRAYS

In principle, it is possible to record multispectral images with simple point detectors. However, array detectors which can simultaneously measure light with multiple detector elements are often required as they can significantly reduce recording time, provide uniformed background and high S/N ratio. High performance array detectors for the UV and visible region (charge couplzed devices (CCD) and CMOS) are readily commercially available with low background, high sensitivity at relatively low cost because they are based on well developed technology. Conversely, infrared array detectors or IR cameras (also known as IR focal plane arrays (FPAs)) were originally developed for military applications and surveillance and have only become commercially available recently. Furthermore, they are based on technology which is relatively less developed than that for UV and visible cameras. However, as demands for these FPAs increase concomitantly with recent advances in material sciences, optics and electronics it is expected that not only newer and high performance FPAs will be available in the near future with much lower cost but also with larger size, better performance, wider spectral response, and faster read out.

Depending on the spectral region, and even in the same region, there are many different types of IR FPAs. They include indium antimonide (InSb), platinum silicide (PtSi), indium gallium arsenide (InGaAs), germanium (Ge), mercury cadmium telluride (HgCdTe) and quantum well infrared photodetectors (QWIPs). In the following section,

characteristics, advantages and limitations of four of the most widely used IR FPAs in IR multispectral imaging, i.e., InGaAs, InSb, HgCdTe and QWIP will be described.

1. InGaAs Focal Plane Arrays

InGaAs/InP is a direct bandgap intrinsic detector that is primarily used for application requiring response in the 0.9 to 1.7 μm region.[23–25] Having low dark current and noise and ability to operate at room temperature have increasingly made InGaAs the FPAs of choice for short wavelength IR detection. Detailed information of the standard $In_{0.53}Ga_{0.47}As/Inp$ detector structure has been previously described.[23–25] Current work has focused on extending cutoff wavelength to 2.6 μm. Highest performance, however, is best achieved when lattice matched at cutoff wavelength of approximately 1.7 μm and grown via metalorganic chemical vapor deposition. InGaAs FPAs with large number of pixels (640×512) and high performance (128×128 InGaAs FPA with room temperature D* value of 1.5×10^{13} cm-$Hz^{1/2}$/W and D* value at 195°K of 11.1×10^{15} cm-$Hz^{1/2}$/W for 1.0 to 1.7 μm range) are commercially available with. By varying the indium content, InGaAs FPAs sensitive to 2.0 μm are now available in 320×240 format.[23–25]

As described in the following section and summarized in Table 2, detection of SWIR can also be achieved with FPAs based on either InGaAs, InSb and HgCdTe. Among the three, InGaAs and HgCdTe can be used at room temperature whereas InSb must be cooled to about 80°K. Both InGaAs and HgCdTe can offer radiatively limited detector performance that translates to the higher possible D*. InGaAs FPA may be the detector of choice, when cost is taken into account and when longest detection wavelength is 1.7 μm.[23–25]

Table 2. Characteristics of different types of materials for infrared cameras.

Material	Bandgap energy (eV)	Wavelength cutoff (μm)	Operating temperature (°K)
In_xGaAs/Inp with $x = 0.53$	0.73	1.7	280
In_xGaAs/Inp with $x = 0.80$	0.49	2.5	270
HgCdTe	tunable	1 to ~18	50 to 250
InSb	0.18	6.89	80
QWIP	tunable	tunable	~40

Table 3. Advantages and Disadvantages of different types of infrared cameras.

Detector type	Advantages	Disadvantages
InGaAs	Good Material & dopants Advanced technology High D* values at room temperature	Limited detection range Difficult to produce uniformed and high performance arrays sensitive for wavelengths longer than 1.7 μm
III–V (InSb)	Good material & dopants Advanced technology Possible monolithic integration	Heteroepitaxy with large lattice mismatch
Quantum well infrared photodetector	Matured material growth Good uniformity over large area Multicolor detectors	Low quantum efficiency Complicated design and growth Limited range within a specifically designed material: Not a broad range camera

2. InSb Focal Plane Arrays

InSb is a semiconductor having a band gap energy of 0.22 eV at 77°K, which is suitable for detection of IR radiation from 1 to 5 μm.[26–30] As a consequence, it is an equally sensitive alternative to HgCdTe for middle wavelength IR (MWIR) applications. InSb is relatively easier to produce than HgCdTe; relatively large diameter InSb wafers can be obtained from single crystal ingots. This capability extends the current InSb technology to larger FPAs than HgCdTe FPA, and thus high quality thermal images with large pixel areas are readily available. As a consequence, InSb is often the FPA of choice for high sensitivity MWIR applications that require good, corrected uniformity.[26–30]

3. Mercury Cadmium Telluride (HgCdTe) Focal Plane Arrays

HgCdTe (commonly pronounced ''mer-cad-telluride'') has been the dominant FPAs the IR region. This due to the fact that the band gap energy of $Hg_{1-x}Cd_xTe$ can be readily controlled by judiciously adjusting its composition. As a consequence, $Hg_{1-x}Cd_xTe$ FPAs cover all spectral bands from the short wavelength IR (from short wavelength IR (SWIR) (from 1–3 μm) to long wavelength IR (LWIR) (from 6–12 μm).

Traditionally, this type of FPA is produced from thin $Hg_{1-x}Cd_xTe$ layers epitaxially grown by liquid phase epitaxy on closely lattice matched CdTe or CdZnTe substrates.[29,30] This technology offers the highest quality epitaxial $Hg_{1-x}Cd_xTe$ layer so far. Its advantages include high sensitivity, ability to select cutoff wavelength at time of manufacture, and high operating temperature. Because of these advantages, HgCdTe often seems to be the FPA of choice for IR detection. In fact HgCdTe FPAs can provide detection from 2 to 26 μm. However, but large arrays have been built only to a cutoff of 10 or 11 μm. Operating HgCdTe at warmer temperatures naturally increases the thermally generated noise. The increased noise also manifests itself as a decrease in dynamic range. Compared to other types of IR FPAs, the biggest drawback with HgCdTe is its instability and nonuniformity problems over large areas due to high Hg vapor pressure during the material growth and problem associated with thermal expansion mismatch. This leads to high costs, delayed schedules, nonuniformity, and unfulfilled performance promises. Furthermore, the problems magnify as cutoff wavelength increases.[29,30]

4. Quantum Well Infrared Photodetectors (QWIP)

As described in the previous section, LWIR (8–12 m) imaging systems traditionally have relied on HgCdTe as the only suitable FPAs material. The advantages of HgCdTe FPAs are well known: tunable cut-off wavelength, high quantum efficiency, and significantly higher operation temperature than many other long wavelength detector materials. However, there are problems associated with LWIR FPAs based on HgCdTe including its instability and nonuniformity problems over large areas, and the difficulty in finding a reliable production.

Long wavelength FPAs have also been developed utilizing superlattices or (multiple) quantum well infrared photodetectors (QWIP).[31] A quantum well technology can be used to construct a detector for a particular wavelength by designing the potential depth and width of the well to produce two states separated by the desired photon energy. A FPA based on quantum well can therefore, be constructed from compositional superlattice structure which is made from thin alternating layers of different semiconductors. The periodicity that the layer structure produces results in a change in band structure in the direction perpendicular to the layers and produces sub-bands. Only photons having energies corresponding to the energy of the sub-bands are absorbed. These sub-bands can be tuned by varying the layer thickness. As a consequence, wavelength range which is detected by this type of FPA

can be appropriately tuned. In fact, researchers at the Jet Propulsion Lab have recently developed a QWIP FPA by alternating layers of GaAs (the well material) and $Al_xGa_{1-x}As$ layer.[31] The wavelength of light that the QWIP responds to can be chosen by varyng the thickness of the layers and the mole fraction x in the $Al_xGa_{1-x}As$ layer[31] These layers are deposited by molecular beam epitaxy for precise control of QWIP characteristics. The GaAs/$Al_xGa_{1-x}As$ material system can be tweaked over a wide range to enable detection of light at wavelengths longer than 6 μm.[31]

Multispectral detection can be achieved by stacking QWIP chips having different bandgap superlattices and connected them with multichannel readouts.

QWIP FPAs push the operating temperature from below 12°K to as high as 40°K, depending upon peak wavelength. However, they may have inadequate quantum efficiency to yield satisfactory D*. In fact, D* values of most QWIP FPAs are reportedly to be in the range 10^{10} to 10^{11} Jones at operating temperature of about 78°K. This is due to higher dark current and lower efficiency. Gunapala estimated that the highest possible D* value of QWIP is about 10^{11} [31]. HgCdTe FPAs, on the other hand, can have D* as high as 10^{14} and 10^{13} at 10 and 16 μm, respectively.[29,30] However, QWIP FPAs can have advantage when they are operated at lower temperature. For example, QWIP is known to have superior performance relatively to HgCdTe at 45°K. Furthermore, HgCdTe FPAs with pixel yield greater than 99.5% cannot be consistently achieved.[29,30]

IV. FUTURE PROSPECTS

Taken together, advantages of the AOTF based multispectral imaging instruments including their instrumental simplicity, low cost and superior performance (fast scan ability, high throughput) make them uniquely suited for applications which are not possible with other spectral imaging techniques. Currently, most AOTF based imaging instruments operates in the near and middle IR region (up to about 5 μm) because they are based on the use of AOTFs which were fabricated from TeO_2 crystal and this crystal is transparent in the 0.4 to 5 μm region (Table 1). This should not limit the applications of these imaging instruments because spectroscopic imaging in the NIR region (up to about 3 μm) has been found to be particularly useful in most cases since it is known that measurements in the NIR region require no pretreatment of samples, are noninvasive and nondestructive. Furthermore, because spatial resolution of multispectral imaging instruments is known to be diffraction

limited, it is expected that spatial resolution is much higher in the NIR region than the middle- and far-IR region.

It is expected that concomitant with the increase in applications of multispectral imaging techniques is the demand for imaging instrument with better performance in terms of sensitivity, detection range, scanning rate and portable. Due to its advantages, applications in the NIR region is expected to be increased substantially, and in this region, it is anticipated that InGaAs camera will gain more popularity compared to InSb and HgCdTe cameras. This is because, in addition to its high sensitivity and low cost, InGaAs camera can be operated at room temperature. Such feature facilitates development of a fully field deployable NIR multispectral imaging instrument for remote sensing and on-line monitoring. While current InGaAs cameras are known to be sensitive only up to 1.7 μm, with rapid advances in material science, optics and electronics, it is anticipated that InGaAs FPAs sensitive up to 3 μm will be available soon. In fact, linear arrays InGaAs sensitive to 2.6 μ are currently commercially available and InGaAs FPAs sensitive up to 2 μm has been reported. The long wavelength IR region (from 8 to 12 μm) is also of particular interest for field measurements and remote sensing since it is immune to the solar flare. It is expected that spectroscopic measurements in this region will increase substantially in the near future because of important development made recently including an AOTF based on Tl_3AsSe_3 which is capable of operating in the 8–12 μm[55] region, and the availability of high performance and fast frame rate HgCdTe and QWIP cameras.

REFERENCES

1. Morris, M.D. *Microscopic and Spectroscopic Imaging of the Chemical State*; Marcel Dekker: New York, 1993.
2. Tran, C.D.; Bartelt, M. Performance characteristics of acousto-optic tunable filter for optical spectrometry. Rev. Sci. Instrum. **1992**, *63*, 2932–2939.
3. Tran, C.D.; Simianu, V. Multiwavelength thermal lens spectrophotometer based on acousto-optic tunable filter. Anal. Chem. **1992**, *64*, 1419–1425.
4. Tran, C.D.; Furlan, R.J. Electronic tuning, amplitude modulation of lasers by computer controlled acousto-optic tunable filter. Appl. Spectrosc. **1992**, *46*, 1092–1095.
5. Tran, C.D. Acousto-optic devices: new optical elements for spectroscopy. Anal. Chem. **1992**, *64*, 971A–981A.

6. Tran, C.D.; Furlan, R.J. Acousto-optic tunable filter as a polychromator and its application in multidimensional Fluorescence Spectrometry. Anal. Chem. **1992**, *64*, 2775–2782.
7. Tran C.D.; Furlan, R.J. Spectrofluorimeter based on acousto-optic tunable filters for rapid scanning and multicomponent sample analyses. Anal. Chem. **1993**, *65*, 1675–1681.
8. Tran, C.D.; Furlan, R.J.; Lu, J. Development of a multiwavelength thermal lens spectrophotometer based on an acousto-optic tunable filter as a polychromator. Appl. Spectrosc. **1994**, *48*, 101–106.
9. Tran, C.D.; Furlan, R.J. Amplitude stabilization of a multiwavelength laser beam by an acousto-optic tunable filter. Rev. Sci. Instrum. **1994**, *65*, 309–314.
10. Tran, C.D.; Lu, J. Characterization of the acousto-optic tunable filter for the ultraviolet and visible regions and development of an AOTF-based rapid scanning detector for HPLC. Anal. Chim. Acta **1995**, 314, 57–66.
11. Tran, C.D. Principles and analytical applications of acousto-optic tunable filters. Anal. Sci. Technol. **1995**, *8*, 101A–108A.
12. Pasquini, C.; Lu, J.; Tran, C.D.; Smirnov, S. Detection of flow injection analysis with pH gradient by acousto-optic tunable filter based spectrophotometry. Anal. Chim. Acta **1996**, *319*, 315–324.
13. Baptista, M.S.; Tran, C.D.; Gao, G.H. Near infrared detection of flow injection analysis by acousto-optic tunable filter based spe Anal. Chem. **1996**, 971–976.
14. Tran, C.D.; Gao, G.H. Characterization of an erbium doped fiber amplifier as a light source and development of a near-infrared spectrophotometer based on the EDFA and an acousto-optic tunable filter. Anal. Chem. **1996**, *68*, 2264–2269.
15. Tran, C.D.; Lu, J. Detection of flow injection analysis by acousto-optic tunable filter based fluorimetry and its application in the determination of solvent polarity. Appl. Spectrosc. **1996**, *50*, 1578–1584.
16. Tran, C.D.; Gao, G.H. Determination of monomethylhydrazine with a novel, high throughput, all fiber near infrared spectrometer based on integrated acousto-optic tunable filter and erbium doped fiber amplifier. Anal. Chem. **1997**, *69*, 1461–1465.
17. Alexander, T.; Gao, G.H.; Tran, C.D. Development of a novel fluorimeter based on superluminescent light emitting diodes and an acousto-optic tunable filter and its application in the determination of chlorophyll a and b. Appl. Spectrosc. **1997**, *51*, 1603–1606.
18. Tran, C.D. Principles and analytical applications of acousto-optic tunable filters, an overview. Talanta **1997**, *45*, 237–248.

19. Tran, C.D.; Huang, G.C. Characterization of the collinear beam acousto-optic tunable filter (CB-AOTF) and its comparison with the noncollinear AOTF and the integrated AOTF. Opt. Eng. **1999**, *38*, 1143–1148.
20. Tran, C.D. Acousto-optic tunable filter: a new generation monochromator and more. Anal. Let. **2000**, *33*, 1711–1732.
21. Miller, P.J. Use of tunable crystal filters to link radiometric and photometric standards. Metrologia **1991**, *28*, 145–149.
22. Miller, P.J. Multispectral imaging with liquid crystal tunable filter. Proc. SPIE **1995**, *2345*, 354–365.
23. Cohen, M.J.; Olsen, G.H. Room temperature InGaAs camera for near-IR imaging. Proc. SPIE **1993**, *1946*, 436–443.
24. Barton, J.G.; Cannata, R.F.; Petronio, S.M. InGaAs NIR focal plane arrays for imaging and DWDM applications. Proc. SPIE **2002**, *4721*, 37–47.
25. Kozlowski, L.J.; Vural, K.; Aria, J.M.; Tennant, W.E.; DeWames, R.E. Performance of HgCdTe, InGaAs and quantum well GaAs/AlGaAs staring infrared focal plane arrays. Proc. SPIE **1997**, *3182*, 2–13.
26. Kimata, M. Infrared focal plane arrays. Sensors Update **1998**, *4*, 53–79.
27. Rogalski, A. Infrared detectors at the beginning of the next millennium. Proc. SPIE **2001**, *4413*, 307–322.
28. Kozlowski, L.J. HgCdTe focal plane arrays for high performance infrared cameras. Proc. SPIE **1997**, *3179*, 200–211.
29. Gopal, V. Key Issues of HgCdTe hybrid focal plane array technology. In: *Physics of Semiconductors Devices*; Kumar, V. and Agarwal, S.K., Ed.; Norosa Publishing House: India, 1998; 729–737.
30. Faraone, L. HgCdTe Infrared detector technology. Kumar, V. and Agarwal, S.K., Ed.; Norosa Publishing House: India, 1998; 721–728.
31. Gunapal, S.; Bandara, S.; Bock, J.; Ressler, M.; Liu, J.; Mumolo, J.; Rafol, S.; Ting, D.; Werner, M. Large format long wavelength GaAs/AlGaAs multi-quantum well infrared detector arrays for astronomy. Proc. SPIE **2001**, *4288*, 278–285.
32. Lewis, E.N.; Treado, P.J.; Reeder, R.C.; Story, G.M.; Dewrey, A.E.; Marcott, C.; Levin, I.W. Fourier transform spectroscopic imaging using an infrared focal plane array detector. Anal. Chem. **1995**, *67*, 3377–3381.
33. Lewis, E.N.; Kidder, L.H.; Arens, J.F.; Peck, M.C.; Levin, I.W. Si: As focal plane array detection for fourier transform spectroscopic imaging in the infrared fingerprint region. Appl. Spectrosc. **1997**, *51*, 563–567.

34. Snively, C.M.; Katzenberger, S.; Oskarsdottir, G.; Lauterbach, J. Fourier transform infrared imaging using a rapid scan spectrometer. Opt. Lett. **1999**, *24*, 1841–1843.
35. Weerd, J.V.; Brammer, H.; Boon, J.J.; Heeren, R.M.A. Fourier transform infrared microscopic imaging of an embedded paint cross section. Appl. Spectrosc. **2002**, *56*, 275–283.
36. Rafferty, D.W.; Koenig, J.L.; Magyar, G.; West, J.L. Fourier transform infrared imaging of nematic liquid crystals. Appl. Spectrosc. **2002**, *56*, 284–287.
37. Scott, W.H.; Bhargava, R.; Levin, I.W. Generalized implementation of rapid scan fourier transform infrared spectroscopic imaging. Appl. Spectrosc. **2002**, *56*, 965–969.
38. Colarusso, P.; Didder, L.H.; Levin, I.W.; Fraser, J.C.; Arens, J.F.; Levis, E.N. Infrared spectroscopic imaging: from planetary to cellular systems. Appl. Spectrosc. **1998**, *52*, 106A–120A.
39. Bhargava, R.; Levin, I.W. Fourier transform infrared imaging: theory and practice. Anal. Chem. **2001**, *73*, 5157–5167.
40. Schaeberle, M.D.; Karakatsanis, C.G.; Lau, C.J.; Treado, P.J. Raman chemical imaging: noninvasive visualization of polymer blend architecture. Anal. Chem. **1995**, *67*, 4316–4321.
41. Schaeberle, M.D.; Kalasinky, V.F.; Luke, J.L.; Lewis, E.N.; Levin, I.W.; Treado, P.J. Raman chemical imaging: histopathology of inclusions in human breast tissue. Anal. Chem. **1996**, *68*, 1829–1833.
42. Kline, N.J.; Treado, P.J. Raman chemical imaging of breast tissue. J. Raman Spectrosc. **1997**, *28*, 119–124.
43. Tran, C.D.; Cui, Y.; Smirnov, S. Simultaneous multispectral imaging in the visible and near infrared region: applications in document authentication and determination of chemical inhomogeneity of copolymers. Anal. Chem. **1998**, *70*, 4701–4708.
44. Fischer, M.; Tran, C.D. Evidence for kinetic inhomogeneity in the curing of epoxy using the near-infrared multispectral imaging technique. Anal. Chem. **1999**, *71*, 953–959.
45. Fischer, M.; Tran, C.D. Investigation of solid phase peptide synthesis by the near infrared multispectral imaging technique: a novel detection method of combinatorial chemistry. Anal. Chem. **1999**, *71*, 2255–2261.
46. Tran, C.D. Visualizing chemical composition and reaction kinetics by near infrared multispectral imaging technique. J. Near-Infrared Spectrosc. **2000**, *8*, 87–99.
47. Khait, O.; Smirnov, S.; Tran, C.D. Time resolved multispectral imaging spectrometer. Appl. Spectrosc. **2000**, *54*, 1734–1742.

48. Khait, O.; Smirnov, S.; Tran, C.D. Multispectral imaging microscope with millisecond time resolution. Anal. Chem. **2001**, *73*, 732–739.
49. Alexander, T.; Tran, C.D. Near infrared spectrometer determination of di- and tripeptides synthesized by combinatorial solid phase method. Anal. Chem. **2001**, *73*, 1062–1067.
50. Tran, C.D. Development and analytical applications of multispectral imaging techniques. Fres. J. Anal. Chem. **2001**, *369*, 313–319.
51. Alexander, T.; Tran, C.D. Near-infrared multispectral imaging technique for visualizing sequences of di- and tripeptides synthesized by solid phase combinatorial method. Appl. Spectrosc. **2001**, *55*, 939–945.
52. Politi, M.; Tran, C.D. Visualizing chemical compositions and kinetics of sol-gel by near-infrared multispectral imaging technique. Anal. Chem. **2002**, *74*, 1604–1610.
53. Morris, H.R.; Schaeberle, M.D.; Treado, P.J. Chemical imaging with tunable filters: methods and applications. Proc. SPIE **1995**, *2382*, 89–94.
54. Turner, J.F.; Treado, P.J. LCTF Raman chemical imaging in the near-infrared. Proc. SPIE **1997**, *3061*, 280–283.
55. Suhre, D.R.; Villa, E., Imaging spectroradiometer for the 8–12 μm region with a $3\,cm^{-1}$ passband acousto-optic tunable filter. *Appl. Opt*. **1998**, *37*, 2340–2345.

MARCEL DEKKER, INC. • 270 MADISON AVENUE • NEW YORK, NY 10016